HIGH RESOLUTION SOLAR PHYSICS BY INTERFEROMETRY: SOLARNET

Luc Damé, Marc Derrien, Mathias Kozlowski and Mohamed Merdjane

Service d'Aéronomie du CNRS, BP 3, 91371 Verrières-le-Buisson Cedex, France
Phone: +33-1-64474328, Fax: +33-1-69202999, e-mail: luc.dame@aerov.jussieu.fr

ABSTRACT

We propose a mission concept allowing very high resolution in the far ultraviolet and ultraviolet, yet not compromising temporal and spectral resolutions. The compact interferometer system proposed for SOLARNET is capable of instantaneous imaging through three cophased telescopes of 35 cm diameter on a one meter baseline feeding a subtractive double monochromator providing wide field of view and high spectral resolution. Comprehensive mechanical and optical realization schemes and image reconstruction scenario have been developed and are presented. One of the major issue, the validity of the use of interferometric techniques (recombination principles, cophasing possibilities), was demonstrated both on a laboratory representative breadboard and directly on the Sun: feasibility of the cophasing of two telescopes on extended reference objects. Furthermore, a complete three telescopes imaging breadboard is now under realization and will be tested in laboratory this summer and on the sky this autumn. These progresses in both the modelisation and laboratory demonstration work truly open the possibility to use and discover from solar interferometers in Space in the short term, i.e. in the ESA F2/F3 framework. With a 1 meter baseline or so, a UV imaging interferometer like SOLARNET will reach a spatial resolution of 0.02" (20 km in the far UV) and a field-of-view of 40" allowing to untangle the confining and dissipating mechanisms and processes from the chromosphere to the corona (the spatial resolution is 40 times that of any previous experiments in Space). This "small" interferometer will also provide the first complete test of interferometric technologies in Space before investing in — much — larger Astrophysics or Earth Observation missions.

Key words: Sun, solar interferometry, high resolution, solar imaging and spectrometry.

1. INTRODUCTION

Back in 1989 we proposed the *Solar Ultraviolet Network* (SUN) a 4-telescopes interferometer for imaging (by rotation of the array as a whole) the fine structure of the Sun and Planets (Damé *et al.,* 1989). This instrument and the Mission it belonged to, SIMURIS (*Solar Interferometric Mission for Ultrahigh Resolution Imaging and Spectroscopy*), eventually completed a First Phase of Study in the context of the Space Station in 1991 (Coradini *et al.,* 1991). Studies were pursued up to 1993 when a smaller version of the interferometer, MUST (*Multi-mirror Ultraviolet Solar Telescope*) was considered for the External Viewing Platform of the Space Station. In parallel, the MUST interferometric concept (5 telescopes on a circular baseline allowing snapshot/instantaneous imaging) was also proposed for a satellite mission (Damé *et al*., 1993a) with some success. SOLARNET is the ultimate simplification of the MUST interferometric imaging concept where the five Ø200 mm telescopes are reduced to three larger ones of Ø350 mm. This simplifies the recombination but, also, provides better imaging by an enhanced coverage of spatial frequencies in the u,v plane. While SOLARNET is yet considered and recommended by ESA for a future mission on the Space Station (with a possible priority on the demonstration of interferometric technologies), it could also be considered as the heart of a larger ESA Mission in the context of F2/F3.

In support to ESA studies CNES engaged, in 92, Research and Technologies (R & T) funds for the realization of a two-telescopes breadboard to demonstrate the heart of the system: the measurement of an absolute phase and the cophasing control of the interferometer.

The breadboard was completed in spring 1994 and by September 1994 a complete laboratory demonstration of the cophasing of two-telescopes on extended objects was achieved (with cophasing performance better than $\lambda/360$). During summer 1995 the breadboard was installed at Meudon Observatory at the “Grand Sidérostat de Foucault” and the first direct cophasing on the Sun was made with a phase control of $\lambda/140$ (Damé, 1996). These cophasing experiments were repeated in 1996 with a better performance: $\lambda/240$. Following these successes we can now sustain that we have the recipe and the cooking skills for the realization of a major instrument for advances in Solar Physics at the beginning of next century.

In the following, we briefly recall the objectives and concepts of the Solar Imaging Interferometer (SOLARNET), explain the constraints imposed by the measurement of a phase over extended objects, briefly present the past and present laboratory and sky results obtained with this first solar interferometric experiment of cophasing on extended objects like the Sun and Planets (see also our other paper in these proceedings). We conclude with a description of the current design and required resources of SOLARNET as it could be implemented either on the Space Station or on a low cost satellite for the ESA F2/F3 mission using the new PROTEUS platform developed by CNES and AEROSPATIALE.

2. SCIENTIFIC OBJECTIVES FOR HIGH RESOLUTION

2.1. The Sun

The relevant minimum observable scale in the solar atmosphere may be of the order of 10–30 km since smaller scales will probably be smeared out by plasma micro-instabilities (such as drift waves). This scale range is comparable to the photon mean free path in the chromosphere. Slightly larger scales can be expected in the corona (though gradient across coronal loops may also be a few km). Altogether this situation is rather fortunate because we have access to higher resolutions in the far UV than in the visible and X-rays (multilayer telescopes are limited to resolutions of 1 arcsec or so). In the UV, the emission lines are generally thin, i.e. not affected by the optically thick transfer conditions (which prevail in the visible and near UV lines accessible from ground) and we can expect to see structures with scales 10 to 30 km. In the visible, thick transfer in the atmosphere blurs the signature of structures and nothing smaller than 70–100 km should be observed. This means that with a single instrument of meter class diameter we have the appropriate, *scientifically justified*, spatial resolution for both the far UV (20 km in the C III line λ117.5 nm) and the near UV (60 km in the Ca II K line λ396.3 nm).

A breakthrough in high spatial resolution observations (20 km is 40 times more spatial resolution than any previous solar instrument in Space) should allow to understand in finer physical details processes like magnetic heating in coronal loops (temperature profiles, time dependence, spatial localization of heating processes) but, also, by access to visible wavelengths, the coupling between turbulent convective eddies and magnetic fields in the photosphere. Another scientific objective is the plasma heating processes and thermal inputs of flares and microflares and their fine magnetic field structures. More details on the scientific objectives can be found Damé *et al.* (1993b).

The SOLARNET objectives are indeed to study the Sun and Planets at very high spatial resolution using spectro-imaging simultaneously in the far ultraviolet (FUV) and the UV.

High spatial resolution is only one aspect since high spectral resolution will also be achieved simultaneously from the photosphere/chromosphere to the transition region and corona (in the SIMURIS payload, this spectral coverage would be further completed by larger-field EUV and XUV imaging telescopes at various wavelengths).

SOLARNET, by access to very high spatial, temporal and spectral resolutions, aims to obtain the measurement capability needed to accomplish the transition from studying *phenomena* to studying *physical processes*. Solar Astrophysics is in a prime position to explain the nature of the physics underlying observed patterns — rather than just "observing" the patterns — because the Sun is sufficiently close that basic physical scales such as density scale height and photon mean free path are in reach of observation. In angular measure, these are a million times smaller for other stars; thus, solar physics requires only a millionth of the baseline needed to resolve comparable physical processes outside the solar system.

The Sun represents an Astrophysics laboratory of huge interest. The solar photosphere is the only place where stellar convection can be observed in detail; the outer atmosphere, pervaded and finely structured by highly intricate magnetic fields, provides a tremendous array of plasma processes, offering much to learn to plasma physicists and astrophysicists alike. The variety of solar research topics that SOLARNET will revolutionize (MHD configurations: fluxtubes, canopies, loops; structure and evolution of magnetic patterns: umbrae, penumbrae, plage, network, grains, fibrils, spicules, prominences; instabilities and eruptive phenomena: jets, bullets, explosive events, flares, microflares; radiation hydrodynamics: granulation, oscillation grains, shocks, extreme limb, plus probably quite a number of structuring agents and dynamical processes that aren't known yet, at scales below the few 100 km resolution) is very large. Nevertheless, they may be grouped together in a single theme, which is defined as the complex entity constituted by a magnetically-active star's outer envelope. In the lower atmosphere, the transition from convective to radiative energy transport causes detailed structuring of the surface layers accessible in the visible part of the spectrum; in the structuring and energy balance of the outer solar atmosphere, a very dynamic plasma best observed in the ultraviolet down to the soft X-ray domain, magnetic fields play a dominant role.

The need to achieve high-resolution solar physics with appropriate diagnostics makes for a specification list of hard-to-meet requirements for a mission:

Very high spatial resolution. The basic scales at which processes are observable is set for the solar photosphere by the photon mean free path, because in optically thick conditions photon travel lengths set the smallest scale at which the emergent radiation is coded by structuring in the state parameters. The basic resolution element one aims for in optically-thick observing therefore measures a few tenths of kilometers. This applies to the visible and near-infrared parts of the spectrum, in which the emergent radiation comes from the photosphere.

For the tenuous outer atmosphere, the situation is very much different because it contains structures that are optically thin in many lines, Lyα being the major exception. In optically thin conditions, the emergent radiation (or absorption) scales with the local extinction and is therefore encoded by structuring at any length scale. The basic physical resolution is therefore set by the actual structuring rather then by radiative transfer. This applies to the ultraviolet and X-ray regimes.

The structuring of the solar atmosphere is dominated by magnetic fields. These are organized in three basic entities which are paradigms of solar MHD modeling. At photospheric levels, the field consists primarily of tiny kilo-Gauss magnetic fluxtubes. They are clustered into the magnetic network, with intermediate field-free areas (“cell interiors'”) underlying the *magnetic canopies*, into which the outward expanding fluxtubes combine together in the low chromosphere. At larger height, clustered tube ensembles join in *magnetic loops*. These have large lengths but contain very steep gradients across magnetic field lines. The latter define the structuring to be resolved in ultraviolet and X-ray imaging; it has kilometer scales or even smaller sizes. Current ultraviolet and X-ray imaging and spectrometry just about show that loops exist, at 1 arcsec or 700 km resolution; to achieve kilometer-scale resolution thus requires orders of magnitude improvement.

Multiband observation. The split between the photospheric regime, observed in the visible, and the outer atmosphere observed at shorter and longer wavelengths requires simultaneous observing in different spectral domains. The photosphere and outer atmosphere must be observed together because of the interplay between them: the structuring and processes in the nonthermal outer atmosphere are to a large extent constrained by the configuring impressed by the convective and oscillatory motion patterns in the photosphere and the sub-surface layers — where the mass is.

Choosing the ultraviolet over the sub-mm and the X-ray over the radio domains is obviously dictated by the much larger resolution obtained per baseline at short wavelengths, the much larger choice of spectral line diagnostics at short wavelengths, and the much clearer signatures of temperature and density structuring at shorter wavelengths.

Selective and tunable spectral imaging. In the ultraviolet, all emission is concentrated in lines which must be separated (Table 1). In the visible, imaging bands must be sufficiently narrow to isolate specific layers of the photosphere. Different ultraviolet emission lines and visible continuum bands supply signals of differing information content, for example supplying height resolution in temperature, density and velocity information (Table 2). Diagnostic application requires that the wavelength bands in which images are obtained can freely be chosen throughout the spectrum.

Two-dimensional spectrometry. Measuring physical state parameters (temperature, density, velocity, magnetic field) requires the use of spectral line diagnostics. In particular, precise Doppler and magnetic field mapping requires measurement of detailed line profile shape variations. Such measurement must be achieved with full two-dimensional resolution.

Photon usage versatility. The large variety of solar phenomena, structures and processes requires large versatility in using spectral imaging and imaging spectrometry. Many small structures evolve very fast, requiring instantaneous imaging; many have linear geometry, however, so that limited field coverage may suffice. For other processes, good signal to noise capability is adamant, requiring longer integration times. Sometimes spatial resolution must be traded for speed; spectral resolution should also be an adaptable parameter.

These requirements can only be met by space observation. Of course, the ultraviolet is only accessible from space; in addition, in space the isoplanatic patch is essentially infinite, providing accessibility to off-set reference sources such as the solar limb for pointing and the disk for cophasing. The SOLARNET mission choice of new interferometric techniques also furnishes research capabilities of interest to Solar System science and Astrophysics and, accordingly, SOLARNET may be seen as a precursor to future developments, both in the context of understanding astrophysical processes and in the context of developing space interferometry at short wavelengths.

Table 1 — Far UV lines for fine structure and dynamical studies

Line	Wavelength (Å)	Te (K)	Specific Interest
C III	1175	70 000	Transition zone
S X	1196 1213	$1.2\ 10^6$ "	Corona (density diagnostic) "
Lyman α	1216	20 000	Coronal loops (+ chromospheric studies in the wings)

N V	1243	1.5 10^5	Flares
Si III	1301	35 000	Density diagnostic
O I	1302 1305 1306	10 000 " "	Chromosphere (but fluorescence with Lyβ) " "
Mg V	1324	2.5 10^5	Active regions & active loops
C II	1335 1336	30 000	Filaments & prominences (evidence of sub-arcsec fine structures)
Fe XII	1349	1.5 10^6	Flares
Fe XXI	1354	1.1 10^7	Flares
O V	1371	2 10^5	Flares (impulsive phase ‘clock’)
Si IV	1394	50 000	Strong line
O IV	1401 1405 1407	1.2 10^5 " "	Transition zone
Si VIII	1440 1445	8 10^5 "	Plages & activity Density diagnostic
Fe X	1464	> 10^6	Hot line: coronal Loops
Fe XI	1467	> 10^6	"
C IV	1548 1551	10^5 "	Strong line: transition zone (ratio –> opacity)
Continuum	1600	4200	Temperature minimum fine structure (Bright Points)
He II	1640	30 000	Sunspots (high chrom. but with coronal contribution)
Mg II k h	2796 2803	4400 — 10 000	Chromospheric studies (from Tmin to the high chromosphere)

Table 2 — Line pairs for density and temperature diagnostic studies

Line	Wavelength (Å)	Ne (electrons/cm^3)	Te (K)
Si VIII	1445/1440	1.0 10^7 – 1.0 10^9	7.9 10^5
S X	1213/1196	2.0 10^8 – 2.0 10^{10}	1.2 10^6
C III	1247/1175	1.0 10^9 – 1.0 10^{10}	70 000
Si III	1312/1301	1.0 10^9 – 1.0 10^{11}	35 000
O IV	1407/1405	3.0 10^9 – 3.0 10^{11}	1.2 10^5

Several concrete examples of the high resolution needs are presented in these proceedings noticeably in the review papers of Schüssler, Chiuderi, Harrison and Marsch and would be of little use to duplicate herein. Though let us mention the opened questions of the threads in prominences (Pojoga *et al.*; 1998, Mein *et al.* 1994; Vial *et al.*, 1989), flare kernels and microflares (Hudson *et al.*, 1994; Porter *et al.*, 1994), loops and corona fine structure (Strong *et al.*, 1994; Priest *et al.*, 1998), polar plumes (Allen *et al.*, 1997), magnetic canopy (MDI/SOHO), flux tubes, etc.

The paper of Priest *et al.* (1998) is particularly instructive. Analyzing the temperature profile of diffuse loops at the limb (Yohkoh data) they inferred that the loops are not heated preferentially near the loop base or near the loop summit, but instead rather uniformly along the loop. In turn this suggests that the most likely mechanism is turbulent magnetic reconnection in many current sheets distributed throughout the loop, meaning small scales of 10-20 km or so.

SOLARNET brings also promising capabilities to non-solar studies requiring high spatial resolution. SOLARNET' photon gathering capacity is modest, but one should note that the Sun is as dim per resolved pixel as any other cool star, specific intensity being the signal measure for image elements rather than irradiance. Following are solar-system scientific objectives of interest for giant and telluric planets, comets and asteroids.

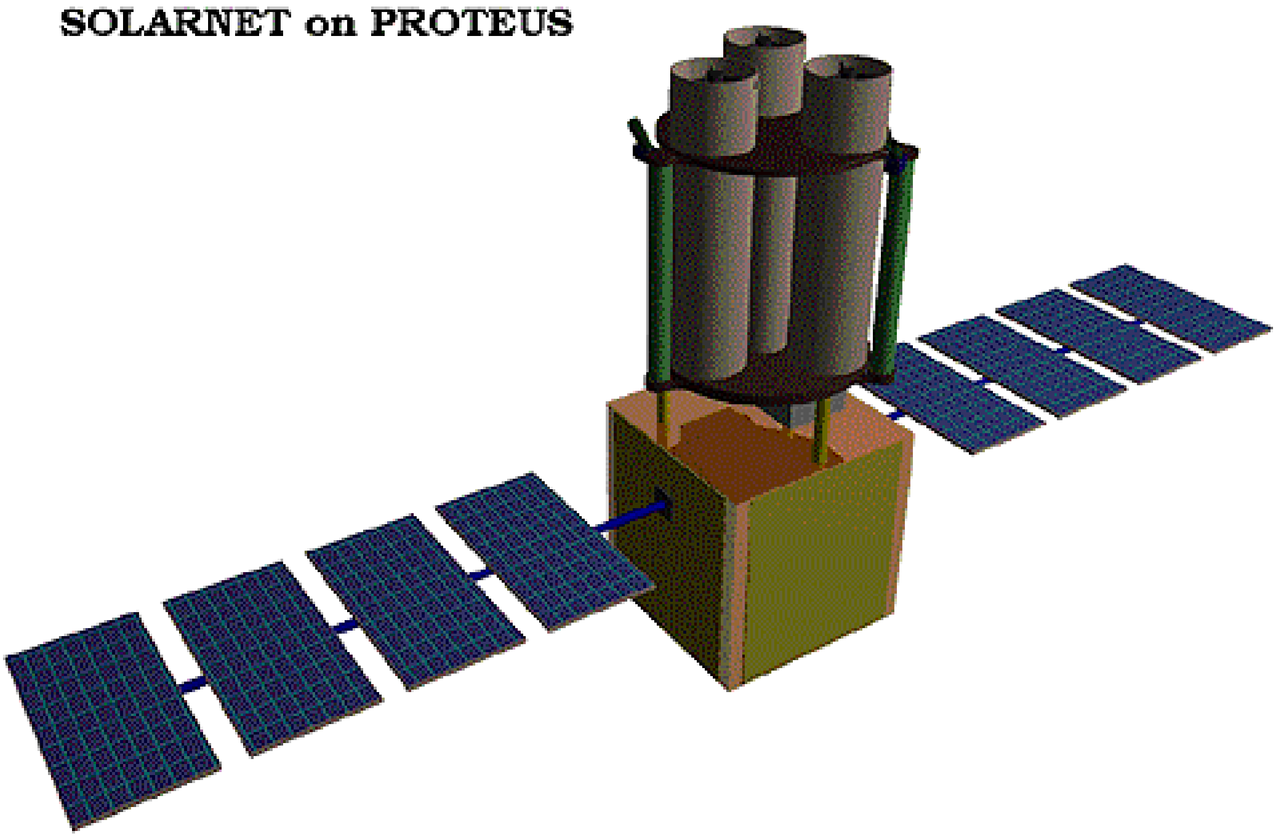

Figure 1. SOLARNET conceptual design (3 telescopes of Ø350 mm on a 1 meter baseline) shown on the PROTEUS platform. This version is considered for flight either as a CNES Intermediate Mission in 2006, as a F2/F3 ESA Mission in 2007/2008, as a NASA MIDEX Mission, or as a multilateral collaboration, e.g. as an ESA SMART complemented by a CNES support (PROTEUS Platform).

2.2. Giant Planets

SOLARNET achieve both high resolution imaging and spectral filtering. At the distance of Jupiter, the SOLARNET instrument has a resolution of 60 km in the UV at 120 nm and 240 km in the visible. At the distance of Saturn, SOLARNET provides maps from the UV to near UV with resolution in the visible up to 100 mas = 700 km. SOLARNET resolves Uranus and Neptune in 40 and 25 resolution elements across their disks in the visible.

Observations performed with SOLARNET will be the UV part of the global, systematic, long-term multispectral monitoring of Jupiter and Saturn global magnetospheric dynamics and upper atmospheres (Prangé, 1992, Zarka, 1992, Prangé and Zarka, 1993 and Zarka *et al.*, 1996).

For the magnetospheres, the aim is to help understanding the relative role of internal processes (plasma sources, rapid rotation) versus external ones (interaction with the solar wind) with respect to the magnetospheric plasma circulation and the auroral processes. This will be done by imaging in the FUV and UV spectral ranges the aurorae (Lyman α, H_2 Werner and Lyman bands, S^{n+} and O^{n+} emission lines, auto and hydrocarbon absorption), of Io (S, O, SO2 in absorption) and of the Io-torus (S^{n+} and O^{n+} in emission), and their correlation to simultaneous observations at other wavelengths, especially radio.

For the upper atmospheres, still poorly documented and understood, the major challenge is to determine the balance between the solar (photon) and auroral (energetic particle) energy input in the upper atmosphere equilibrium, and their effect on the planetary thermospheric dynamics, chemistry and energetics (Emerich *et al.*, 1996, Sommeria *et al.*, 1995). The FUV-UV spectral range is the most suitable one for remote sensing of the pressure levels corresponding to the upper atmosphere (Lyman α, H_2 Werner and Lyman bands in emission, hydrocarbons and H_2O in absorption).

For Jupiter's magnetosphere, the objectives include :

- identification and monitoring of auroral precipitation regions in the magnetosphere through FUV imaging, including the mysterious tiny auroral spot associated with the volcanic satellite Io; by mapping these features up the magnetic field lines, the regions in the deep magnetosphere where auroral processes occur will be identified and their temporal evolution followed;

- determination of the nature and energy of precipitating particles through the interpretation of UV images at high resolution in several spectral ranges using newly developed models of H and H_2 excitation models with radiative transfer effects (Sommeria *et al.*, 1995, Rego *et al.*, 1994, Prangé *et al.*, 1995), search for sulfur and oxygen lines), and subsequent characterization of auroral processes (role of field-aligned currents, discrete versus diffuse aurorae);
- study of the regimes of energy release through correlation studies between the variations of the Io torus, auroral activity (UV, IR, Radio), and solar wind conditions, which are expected to exhibit a large range of different time scales from a few minutes to months and years;
- study of the Io flux tube coupling with Jupiter's ionosphere, through correlations of UV and IR emissions at the Io flux tube footprint and radio decameter emission along it;
- structure of the Io plasma torus, its asymmetries and time variations (in correlation with other magnetospheric fluctuations), which can be revealed by complementary UV (S^{n+} and O^{n+}) and radio (propagation of decameter waves through the torus, and its kilometer-wave emissions);
- study of the escape of material from Io and its torus, of plasma transport from the Io torus to the magnetosphere, and of large scale magnetospheric convection;
- monitoring/imaging of Io's surface and neutral corona (S, O, SO_2) through their FUV/UV signature and relation with Io's variable volcanic activity monitored in IR (ground-based).

Saturn's magnetosphere objectives include:

- monitoring of the poorly studied auroral UV emissions (only observed by Voyager and a few times in the FUV with IUE) : location and time-variability
  - ⇒ in relation with solar wind variations;
  - ⇒ on the long-term for detecting a possible seasonal variation and making the link between Voyager and Cassini measurements;
  - ⇒ versus rotation for constraining further the determination of the magnetic field anomaly;
- search for nitrogen lines of Titanogenic origin in the auroral emissions and tentative imaging of species in the magnetosphere itself (OH, discovered by HST); this would provide insights on the plasma chemistry and transport, on the auroral processes in the vicinity of satellites and tori, and on the effect of ring material in the inner magnetosphere.

The dynamics and energetics of Jupiter and Saturn upper atmospheres is poorly understood. Voyager and IUE observations have revealed anomalously bright FUV airglow (H, H_2) and high temperatures. This can presumably be associated with the huge energy input in the polar aurora, particularly for Jupiter (up to 10^{14} W), suggesting that the equilibrium of Jupiter and Saturn's thermospheres is thus presumably controlled by auroral processes, a situation opposite to the case of the Earth. Very recent high resolution results from HST confirm the high degree of disturbance of the Jovian atmosphere from the auroral region (Pallier *et al.*, 1997) down to the equator (Emerich *et al.*, 1996, Ben Jaffel *et al.*, 1993) presumably through a complex supersonic thermospheric circulation pattern (Sommeria *et al.*, 1995). The polar region of Jupiter and Saturn are also covered by a thin layer of polar hazes (Connerney *et al.*, 1993) attributed to ion-neutral chemistry under energetic particle precipitation.

Long-term survey of the planetary UV dayglow would include the following Jupiter and Saturn's atmosphere objectives:

- study and monitoring of the auroral atmospheric structure at high spatial resolution through the distribution of the species column densities above the auroral sources, including determination of the temperature though temperature sensitive H_2 lines
- simultaneous study and monitoring of the mid-latitude/equatorial "bulge" atmospheric structure with the aurorae using high resolution maps of the Lyman α emission to detect the thermospheric winds paths, the small scale turbulence cells and their relationship with the auroral input and solar cycle
- mapping of the polar haze at various UV wavelengths in order to determine the composition of the structure and composition of the aurorae-induced species and aerosols through modeling of their absorption and diffusion properties (radiative transfer models).

Expected results include:

- Origin of auroral processes at Jupiter; nature, energy and localization of precipitations; magnetospheric circulation, current systems, and time-variability; role of field-aligned currents in the generation of aurorae compared to pitch-angle scattering;
- Nature of the Io flux tube / auroral ionosphere coupling;
- Structure of Io plasma torus, asymmetries, time variations (in correlation with other magnetospheric fluctuations); transport of plasma and energy from the torus to the magnetosphere;
- Solar wind control on magnetospheric processes (degree, short-term, long-term); on Io torus;
- Origin of the variations of Saturnian aurorae (short-term & long-term behavior);
- Solar wind control on the (UV) auroral activity at Saturn;
- First comparative study of the magnetospheres of Jupiter and Saturn, observed simultaneously;
- Interaction of solar wind coronal mass ejections with the magnetospheres of Jupiter and Saturn;
- Excitation mechanism of the H_2 dayglow; correlation with the time variability of the solar

FUV/UV flux and/or with the auroral activity; interaction between the upper atmosphere of the giant planets and their ionized environment (ionosphere, magnetosphere);

- Interpretation of the Lyman-α and helium resonance scattering emissions; of the Lyman-α bulge of Jupiter; monitoring of its long-term variability and correlation with solar and auroral activity; determination of their role as a diagnostic of the upper atmosphere;
- Dynamics and energetics of the upper atmosphere and ionosphere of the giant planets; circulation patterns; ion-neutral aurora-induced chemistry.

Multispectral correlations. Multispectral correlations will be performed with ground-based IR (Jovian aurorae), visible (Io torus) and radio decameter (>10 MHz, in Nançay) observations, with Wind and Ulysses data (kilometer to decameter-wave radio emissions and solar wind parameters) and, hopefully, with a dedicated radio satellite in the 0.1-10 MHz range.

Observations in the radio range are especially complementary to UV magnetospheric observations. The emissions occur along (auroral) magnetic field lines and in Io's torus. They lack spatial resolution but carry information on the energy and distribution function of precipitating electrons (keV range), the magnetic field topology, the evolution of "hot spots" in Io's torus, and the torus electron content.

Correlations between UV and Radio (and IR) are especially important for the determination of the type of aurora observed, the energy budget of precipitations in the auroral regions or Io flux tube, and for deducing the efficiencies of the various steps leading to electromagnetic emissions (energy spectrum of accelerated particles, collisional excitation, joule heating, wave-particle interactions). At Jupiter, multispectral observations will allow to study the Io flux tube/ionosphere coupling, the structure, asymmetries and time variations of Io's plasma torus (in correlation with other magnetospheric fluctuations), and the transport of plasma from the torus to the magnetosphere.

Importance of long-term continuous observations. Previous correlation studies used very discontinuous UV data (IUE spectra or HST images), together with more continuous radio (ground-based) observations. Continuous observations will give access to the variations of magnetospheric (auroral and torus) parameters with planetary rotation (linked to the asymmetries of the planetary magnetic field), solar wind interaction, aperiodic storm-like energy releases, as well as long-term (possibly seasonal) variations. Continuity in the long-term monitoring of the Jovian and Saturnian magnetospheres (from Voyager, Ulysses and Galileo, to Cassini, covering thus >2 solar cycles and 2/3 of Saturn's orbital period) is especially important for the search of seasonal effects in the magneto-ionized environments of Jupiter (orbital period = 11.9 years) and Saturn (= 29.5 years). Remote observations from the Earth's vicinity can be advantageously combined with in-situ measurements by Galileo and/or Cassini (or future planetary orbiters), but they will also provide unique global and continuous informations, not in the scope or capabilities of in-situ missions. For example, the auroral activity of Jupiter and Saturn will be studied simultaneously for the first time, allowing for a comparative study of their magnetospheric dynamics and of their response to solar wind fluctuations, relative to that of the Earth's magnetosphere.

Additional objectives. The special magnetospheric activity of Mercury (substorm-like) and its surface-magnetosphere coupling, unique in the Solar System could also be studied with SOLARNET. The need for high spatial resolution in this case has been highlighted in Prangé (1992), as well as the need for line of sights too close to the Sun for most of the classical planetary dedicated designs.

All spatial scales can be observed in the Martian surface and atmosphere, down to a resolution limit of 40 km in the visible and 10 km in the UV. Structures such as volcanoes or Valle Marineris can be resolved spatially, and investigated in wavelength bands allowing to distinguish structures of geological and mineralogical interest. Also, seasonal surface and surface/atmosphere active processes effects related to the dust storms and frost covers can be monitored. Products and ingredients of the photochemical cycle can be observed at high spatial resolution. This is the case for OH emission at 308 nm or also the 0_3 UV absorption, which can be observed and monitored as indicators of stratospheric H_20 content.

2.3. Comets and Asteroids

SOLARNET will contribute to the study of minor bodies in the solar system by obtaining very high resolution images from the UV to visible. During a 3 years mission, at least 40 asteroids will be seen with a size larger than 75 mas. The resolution of SUN in the visible (80 mas at 400 nm and 25 mas in the UV), will be quite adequate. The 10 larger asteroids with size larger than 250 km (540, 600 and 1016 km for Vesta, Pallas and Ceres) have a diameter at opposition larger than 200 mas in the asteroid main belt (cf. Table 3). They can be mapped with a significant resolution in different bands of chemical and mineralogical interest. Detailed surface features, surface composition and shapes will be measured.

The irregular shape of asteroids will be measured for those smaller than 200 km, whose stresses have not been overcome by gravity. At the resolution of SOLARNET, asteroids in the main asteroid belts can be resolved down to sizes of 15-70 km. A few small bodies approaching the Earth from the Apollo-Amor family can be resolved down to the kilometer size range. This may be an important tool in the process of identification of the Near Earth Objects. It is also worth insisting on the extreme diversity of asteroids and Kuiper objects (Levasseur-Regourd *et al.*, 1996, Hanner *et al.*, 1994) for which multiple discriminating observations would be extremely valuable. This was confirmed by the recent results of Mathilde flyby (Yeomans *et al.*, 1997; Veverka *et al.*, 1997).

Tunable 10 nm broadband fluxes can be measured for a main belt asteroid using the Double Monochromator of SOLARNET with 1000 counts per 25 mas = 20 km resolution element per 15 minutes of observation. In the filter channel 130-300 nm, the counts will be 20 times more (10000 cts in 15 minutes), allowing high signal to noise mapping. The ultraviolet allows investigation of the OH 306.4 nm and the Lyman Alpha 121.6 nm emission from dormant comets with remaining activity.

In cometary research, major information will come from rendezvous missions to individual comets such as Wirtanen that Rosetta will visit in 2011. In 10 years many scientific topics of interest can be addressed. Although 3 comets have been flown by (Giacobini-Zinner, Halley, and Grigg-Skjellerup), and 3 others extensively observed recently (Shoemaker-Levy 9, Yakutake, Hale-Bopp), no information is available on the densities, composition and structure of cometari nuclei. Coarse information on the nucleus shape would provide clues to the aggregation processes and tensile strengths of a significant variety of nuclei. For understanding the formation of coma jets, dust and plasma tails and meteoroid streams, high angular resolution is required. Observations of many comets allows to gather data on several classes of comets. For the nearby ones, the nucleus will be resolved down to kilometer sizes (20 km at distance 1 AU from Earth). The fragmentation of comets approaching from the Sun can also be observed. By selecting bands of mineralogical or chemical spectral signatures, the surface distribution can be derived for the larger comet nuclei. Also, difference in centroid positions of comet nuclei at different wavelengths can be measured with a sub-kilometer accuracy on nuclei brighter than 14 magnitude. In association with photometric rotational modulation, this would allow coarse surface mapping.

The brightest emission lines of the daughter products of water (H, OH and O) are in the UV. SOLARNET can observe these products near the nucleus. The structure of jets of dust and parent molecules can be followed down to the nucleus, and the activity distribution can be mapped. These can be compared to the highest resolution images that can be obtained in the UV. The inner coma has a very complicated spatial distribution. Gas and dust leave the nucleus both by general diffusion and in jets. The dust can be distinguished from the gas by taking images at wavelengths that do not correspond to the gas fluorescent bands. These allow measuring the spatial density of the dust and the size distribution as a function of distance from the nucleus in the jet and non-jet regions. The coma gas leaves the nuclear region at 0.5 km/s. Gas molecules are dissociated into daughter products H, D, OH, C_2, C_3, CO, S_2, SO, CO_2, CN, C, S, CS. The different Swan bands of the hydrocarbons can be selected for imaging with SOLARNET. Cometary emission features of interest include for instance OH 306 nm and Lyman Alpha 120 nm (e.g. for comet Bradfield with respective flux 200 kR and 50 kR, Feldman 1982), CS 257.6 nm, CO_2^+ 289 nm and CN 388 nm. The variation of their fluxes and distribution can be measured as a function of heliocentric distance. Dust is also a source of gas by evaporation of their constitutive "CHON". Recent observations of Hale-Bopp have shown that looking at bright comets allow to discover near the nuclei, new cometary molecules. With its high resolution SOLARNET has certainly a large discovery potential.

The study of the composition of gas and dust emitted by the cometary nucleus will allow to characterize the nucleus emission rate, dynamics and surface distribution. Such studies are feasible as a function of heliocentric distance for different categories of comets. On the average, 30 comets are discovered or recovered on each year; besides, some comets (e.g. Encke) are permanently observable. The narrow band imaging capabilities of SOLARNET allow to build a data base on the diversity of the inner coma. It would also provide unique information on the composition of the ices and dust particles on the nucleus surface. Finally, it could give some hints about the shape, activity, origin and evolution of the cometary nuclei.

Table 3 — Asteroids of the Main Belt that could be mapped by SOLARNET

Number	Name	Diameter (km)	half-axis (ua)	Diameter (mas)
1	Cérès	914	2.767	711
2	Pallas	522	2.771	405
4	Vesta	500	2.362	505
10	Hygeia	430	3.144	276
511	Davida	336	3.178	212
704	Interamnia	334	3.062	223
52	Europa	321	3.097	205
15	Eunomia	275	2.644	227
87	Sylvia	275	3.486	(150)
16	Psyché	264	2.922	(188)
31	Euphrosyne	248	3.156	(158)
65	Cybèle	246	3.429	(139)
3	Juno	244	2.670	201
324	Bamberga	242	2.683	(198)
107	Camilla	236	3.488	(130)

3. WHY AN INTERFEROMETER?

If the need for high spatial and spectral resolutions is commonly agreed, the question left is: why an interferometer and not a single-dish large telescope? The first answer is that the required measurement needs exceed conventional instrumentation possibilities. A 1 m telescope diffraction-limited in the far UV is, in practice, exceedingly difficult to construct. And, even assuming that such a perfect 1 m telescope could be built for the far UV, it would be more costly and difficult to control and assemble than an interferometer.

In fact, the Michelson interferometric approach represents significant advantages over diffraction-limited large telescope imaging and the "natural" choice for high resolution is the interferometer for several reasons:

- size, mass and cost: between an interferometer of 1 m baseline and height 1.3 m and a classical monolithic telescope of nearly 4 m height (cf. Fig. 2), the mass, difficulties and launch cost will explode.
- Figure and ripples. Telescopes larger than Ø400 mm cannot be polished to the specification of $\lambda/8$ (wave, peak-to-valley) at Lyman α (121.6 nm) while small ones can. The Hubble Space Telescope, a 2.4 m mirror, even with a perfect figure, would still be a factor 10 away (0.1 arcsec rather than 0.01 arcsec) from its diffraction limit in the far UV (Damé and Vakili, 1984) due to the residual ripples left on its surface by the polishing process (tools of 10 cm or so).
- Adaptive optics. Interferometry requires to control the residual optical path delays between telescopes but this, consequently, guarantees a perfect output wavefront suitable for diffraction-limited imaging. Adaptive optics is not an alternative to obtain the correct figure precision of large mirrors or to control the resulting errors, because of the extended field-of-view, the time response required and the severe in orbit thermal cycling. Note that aligning a segmented mirror requires 6 degrees of freedom and a control of the distance between the primary and secondary mirrors. Further, this very complex control loop — which is not required with an interferometer made of small telescopes since, beside fine pointing needs, only one degree of freedom is required: the phase control — does not work properly on *solar extended objects.*
- Active pointing. Only small telescopes are necessary and their small secondary mirrors can act directly as active pointing mirrors, without requiring intermediate optics for this purpose.
- Small telescopes means small beams, easier recombination, lower coast of optics (and better quality), simpler focal instrumentation, etc.

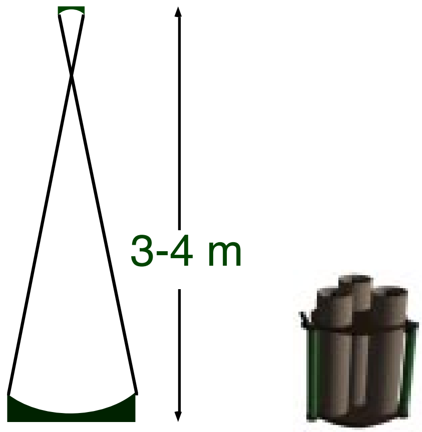

Figure 2. The evident size, mass, alignment control... advantages of an interferometer of 1 m over a monolithic telescope of the same diameter.

Altogether, the modest baseline required to obtain major scientific results and the simplified control of an imaging interferometer (which doesn't need an absolute metrology like complex astrometric missions) result in very reasonable cost and mass which open solar (and planetary) interferometry programs to the medium size satellites programs — like the CNES Intermediate Missions on the PROTEUS Platform — or to the limited accommodation capabilities of the International Space Station. SOLARNET, completed with XUV telescopes and larger field instruments, is the baseline of the Reduced SIMURIS Payload adapted to small platforms and satellites (cf. Table 4). XUV spectrometers and solar irradiance monitoring instruments could also be envisaged for completeness as a Solar Observatory. For the Space Station, SOLARNET alone could be envisaged with both scientific and technical objectives (demonstration of a complete interferometric system in Space).

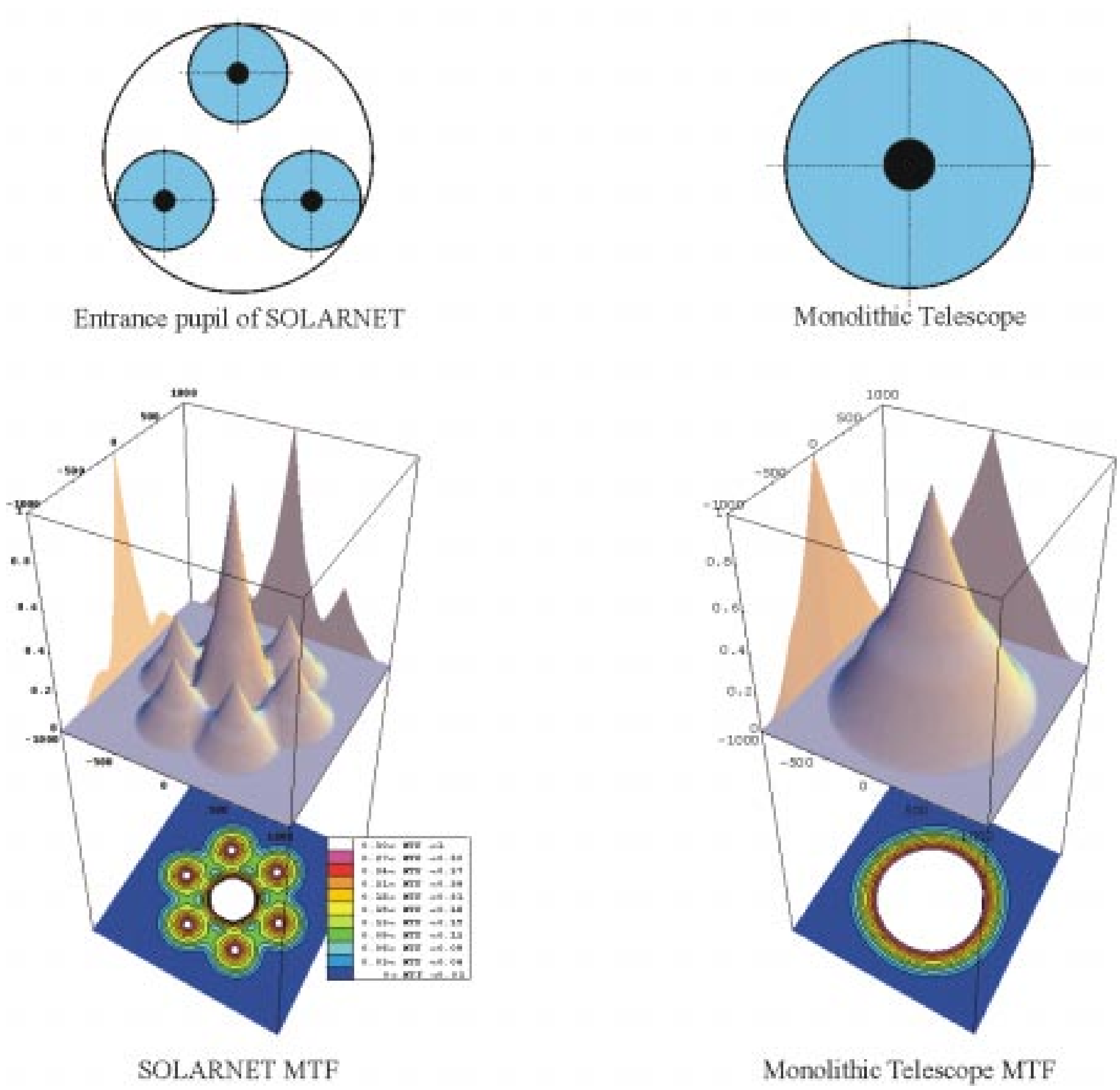

Figure 3. Comparison of Modulation Transfer Functions (MTF) between a monolithic telescope of 1 meter diameter and an imaging interferometer of the type of SOLARNET with 3 Ø350 mm telescopes on a circular baseline of 1 meter or so. One can notice that SOLARNET has a response at low and high spatial frequencies comparable to the monolithic telescope. The monolithic telescope is superior only in the medium frequencies range and, even in this case (an even if deeps are as low as 7% of the peak), ALL THE SPATIAL FREQUENCIES ARE COVERED by SOLARNET. This unusual, excellent, instantaneous spatial frequencies coverage, makes that , alike a monolithic telescope, SOLARNET will directly provide a 2D image at high resolution in only one single exposure. No need to rotate or rearrange the array, all spatial frequencies being present at once. And, by a simple, direct, deconvolution of this recorded image/interferogram, will the image of the object be recovered.

4. IMAGING WITH A STABILIZED AND COMPACT ARRAY

Assuming that we are capable of controlling to a certain extent the OPD (and the pointing) between the telescopes of the array, we can register the interferograms (images on which are superimposed the fringes) and reconstruct the high resolution images. Though, the method has to be specific since, when the finite size of the individual telescopes is accounted for, the SOLARNET instrument samples a full range of spatial frequencies ranging from zero up to the maximum baseline of 1 m. This completeness is unusual in conventional interferometry and has more in common with the Fourier plane coverage of the Multi-Mirror Telescope (MMT). It means that the imaging capabilities of the instrument are *excellent*. While these spatial frequencies are potentially accessible, there are a number of different schemes for measuring them since measurement of the fringes is possible in both image or pupil planes. In the image plane, it is necessary to sample the fringes for a given pair of telescopes for all independent positions in the image (every half-Airy disk in practice), while in the pupil plane the equivalent scheme is to measure fringes for a pair of telescopes for a number of different spatial offsets or shears between the pupils. In radio-astronomy, the image plane scheme is used for making images of objects larger than the Airy disk of the elements of an interferometric array, each image plane point being sampled sequentially. However, to image a FOV of 40 x 40 arcsec^2 would require thousands of separate fringe measurements for each pair of telescopes. Clearly, then, a superior method is to place *all these fringes on one detector at once*. We then require to interfere light from all telescopes on a detector covering a FOV of 40 x 40 arcsec^2 with a spatial sampling of 12 mas (to achieve diffraction-limit — 24 mas — of the 1 m array at Lyman α). The image obtained on the detector *instantaneously* is the true object convoluted with the instantaneous point spread function of the instrument (plus photon noise, *etc*.). But this direct image can be restored by inverse methods techniques as we will show.

Since the cophasing will not to be perfect, residual independent errors will impede the possible quality of the image reconstruction. Nevertheless, results of compact arrays are far superior than diluted ones to reconstruct images in these conditions because they allow complex structures and extended FOVs. This was confirmed and studied independently by Cornwell *et al.* (1993, the ‘homogeneous’ array concept) and our studies (Damé and Cornwell, 1992, Damé, 1993, 1994). Millimetric arrays (e.g. like the MMA project) which are sensitive to phase errors and aiming at extended FOV are also oriented towards circular and compact array configurations.

Extensive simulations have been carried for the SUN and MUST interferometers to establish that excellent images can be obtained from compact optical arrays despite errors in visibility (contrast) data, caused by residual beams’ mispointing and residual phase errors between beams. The results are, naturally, very similar for SOLARNET and, so, please refer to Damé (199', 1993) for illustration of the influence of flux level, phase and pointing errors on image reconstruction. These simulations indicate, in particular, that image dynamics is directly linked to the flux level (N ph/s/pixel) and more or less limited to $\sqrt{N}$, and that when phase errors are ≤ λ/6 (10° phase error) and pointing errors are ≤ 20 mas, reconstructed images are diffraction-limited to the resolution of the array (dynamical range is about 400). Though, it is certainly worth to achieve the best cophasing since the higher dynamical ranges (> 1000 — when flux is available) are not accessible without nearly perfect cophasing.

However, and even if these simulations are nice and instructive, it is worthwhile to give a direct "taste" of the imaging capabilities of an interferometer. For this we choose a "common" object, like a cat, and submit it to imaging by one of the SOLARNET telescopes alone (Ø350 mm), a monolithic telescope of 1 m, and the SOLARNET interferometer of 3 x Ø350 mm telescopes on a 1 m or so circular baseline. The results are straightforward (cf. Fig. 4) and show — let us call a cat a cat... — that a compact interferometer of the type of SOLARNET is strictly equivalent to a monolithic telescope when phased (and for the same photon gathering: this implies a factor 2 more for the exposure time). Note also that if the monolithic telescope was not processed (proper deconvolution), then its spatial resolution would be inferior to the one of the interferometer! Finally, one should also notice the significant improvement in the geometry restitution of structures brought by the factor 3 (9 pixels averaged) between the SOLARNET array and a single Ø350 mm telescope (cf. the eyes of the cat for example).

In practice, this shows that the exceptional — ‘compact’ — u,v plane coverage of SOLARNET, and its real-time metrology and compensation schemes of the pointing and phase errors, allow imaging capabilities of extended and complex objects similar to those of a single-dish, monolithic, telescope.

5. COHERENCE AND COPHASING

To study the ultimate fine structure of the Sun, a solar interferometer needs to image an extended field-of-view (FOV) covered with complex structures. And, since many structures of interest are evolving rapidly (in a few seconds or even less), this imaging cannot be achieved by classical long-baseline interferometry techniques where fringes' visibilities are measured sequentially.

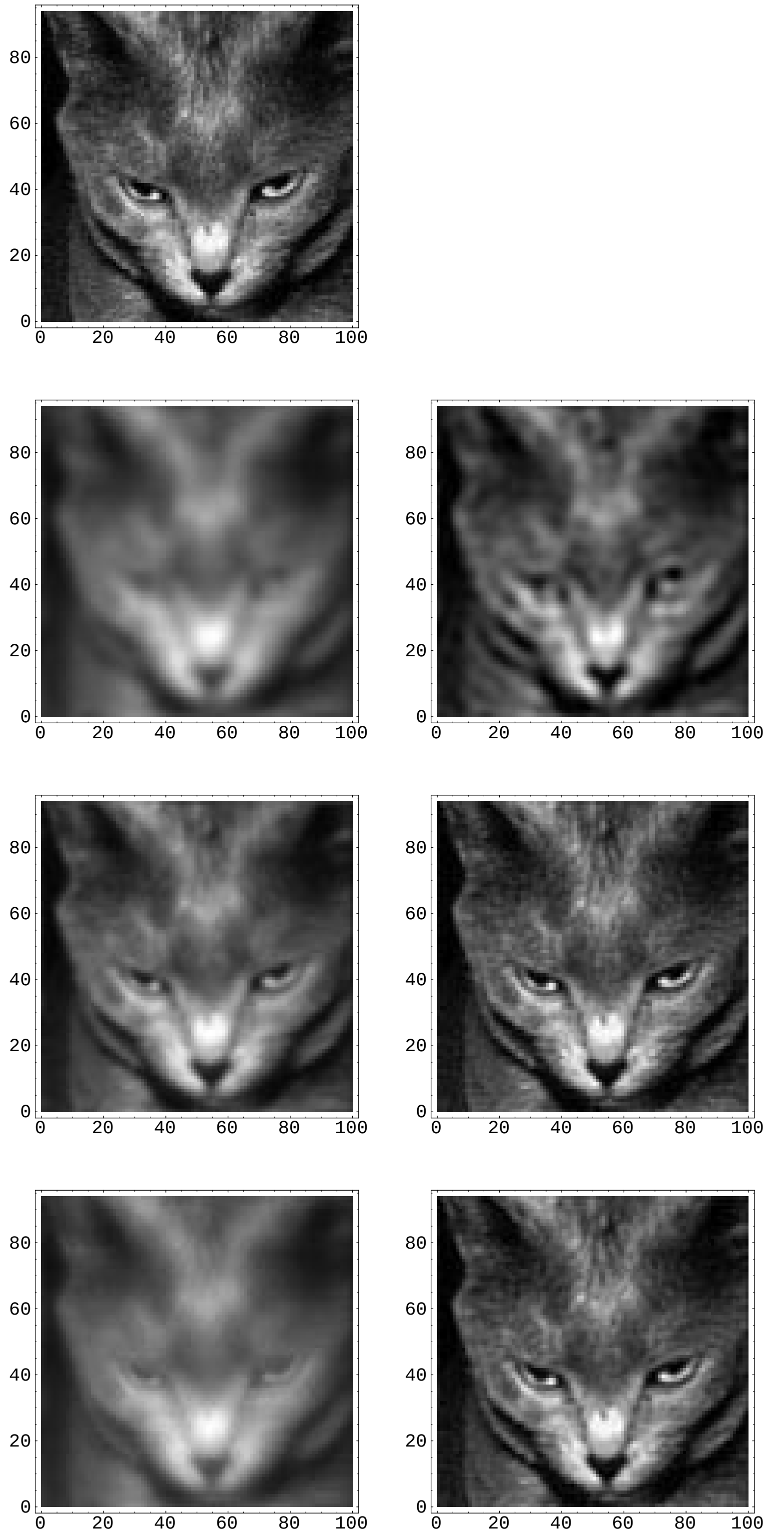

Figure 4. Illustration of a simple deconvolution with SOLARNET and comparison with a "small" telescope of Ø350 mm and a "large" of 1 m. From the reference image (Top left) we obtain (2nd line) the image of the "small" telescope (left) and its deconvolution (right); the one of the "large" telescope and its deconvolution (Center) and (Bottom) the image given by SOLARNET and its direct deconvolution (divided by the optical transfer function). Notice the absence of differences between SOLARNET and the large monolithic telescope and the meaning of a factor 3 in resolution between the small telescope and SOLARNET (cf. the "cat's eye" identification).

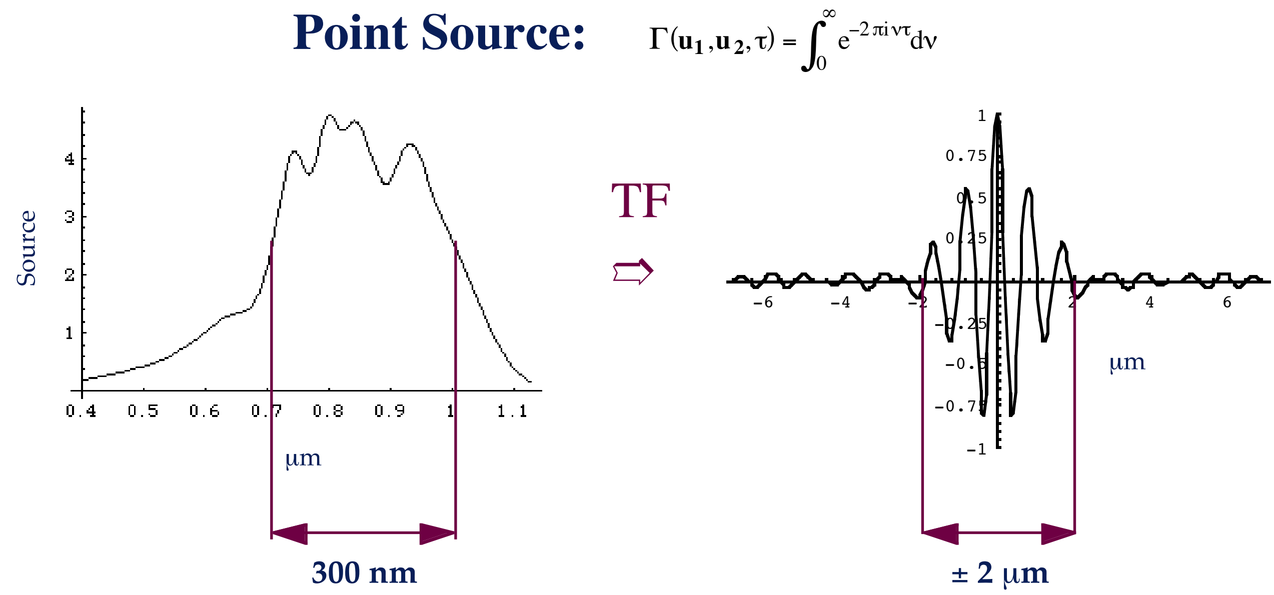

Figure 5. Assuming a large spectral bandpass for the source (300 nm or so at FWHM), the resulting coherence length is short (~ 2µm) resulting in 5 major fringes on an optical path of ± 2 µm.

These constraints (FOV and time resolution) prompt to design an interferometer with instantaneous imaging capability i.e., first, to the choice of a compact array. By compact is meant that the spatial frequency coverage of the array is comparable to a single dish telescope in one fundamental aspect: complete coverage of spatial frequencies, i.e. there are no zeroes in the modulation transfer function of the array. Image restoration is, in this case, as we have just seen, based on a direct deconvolution. A central issue for interferometric imaging is, therefore, a proper (i.e. compact) configuration of the array.

The other important requirement is to control the residual optical path delays between the different telescopes to a fraction of a wavelength, i.e. to *cophase* the interferometer. This allows all the recorded fringes to be used *instantaneously*, since not affected by a significant phase problem (thus allowing a robust image reconstruction approach). The consequence of importance brought by this cophased approach is that, permanently, we have the insurance of a near perfect wavefront (stable transfer function), the telescopes of the array being controlled to their optimum phase position.

5.1. Cophasing principle

The major conceptual choice of our interferometric approach is to cophase the array. By "cophase" we mean real-time control of the phase differences between the telescopes, i.e. constant monitoring of the equality of the optical path-lengths traveled by the different beams. The result of this cophasing is that the transfer function of the system is stable. Cophasing has a sound justification since only cophased arrays can integrate light, i.e. benefit from long exposures and, thus, from a better signal to noise ratio. The measurement of an absolute phase on an extended object is not straightforward and we will first recall some basic notions of coherence.

In our approach of cophasing, the fringes formed in the reference interferometer are obtained by superimposing the pupils. We have direct interferences point-by-point on the pupil and, in each case, the baseline is exactly the same. This is a Michelson case (not a Fizeau case which is obtained when an angle is introduced between the two beams during the superimposition).

On the contrary to a point source (e.g. a simple star) for which the mutual coherence function (i.e. the fringe pattern as a function of time or, in practice, as a function of the position of a delay-line) is simply the result of the integral over the spectrum (cf. Fig. 5), when the source is extended and with a large spectral bandwidth, spatial effects are added to the temporal ones; this is the general coherence case for the computation of the mutual coherence function where we integrate the source emission spectrum $E(\mathbf{x},\nu)$ over the frequency domain and the source extension:

$$\Gamma\left(\vec{\mathbf{u}}_1,\vec{\mathbf{u}}_2,\tau\right)=\int_0^\infty e^{-2\pi i\nu\tau}d\nu\int_\varsigma \frac{E\left(\vec{\mathbf{x}},\nu\right)e^{2\pi i\nu(R_2-R_1)/c}d\vec{\mathbf{x}}}{R_1R_2}$$

where ν is the frequency and τ the time delay (expressed in seconds). Other notations are explained in Damé (1994).

We have evaluated this triple integral for different source extension ζ (from 0.15" to 0.6") using the measured source spectrum of our laboratory source ($\Delta\lambda \approx 300$ nm). 0.6" is the classical spatial resolution ($1.22\lambda/D$) of a 350 mm telescope at λ800 nm while 0.4" is about the spatial resolution (λ/B) of the interbaseline on which the contrast is measured (525 mm), i.e. the value at which the contrast becomes zero. As can be seen from Fig. 5, 0.15" and 0.3", the two first values, are perfectly acceptable source' sizes since the fringe contrast in that case is 61% and 22% while 0.35", 0.45" or 0.6", the three other values of the source used in this simulation, are harder to use, not so because of the value of the contrast, than because of the required algorithm to localize the central fringe without ambiguity (the central fringe may not be the most important one and it can even be negative). Note that the coherent fringes are present on only ± 2 µm (coherence length of ~ 2 µm).

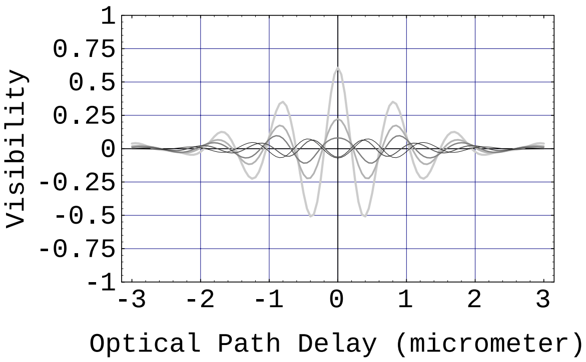

Figure 6. Fringe visibility as a function of the path delay (in µm) when the source size varies from 0.15 to 0.6". For reference sources' sizes less than the spatial resolution of the interferometer, the contrast of the central fringe can be very good: ≥ 60%.

Because of the limited baseline (525 mm) between nearby telescopes (Ø350 mm), the eventual complexity of the source has only a negligible influence on the position of the central fringe which measurement can therefore be considered absolute. However, when telescopes are small compared to the baseline (classical stellar case) this assumption may not be true anymore (see, for example, Annex 1 of Damé, 1994).

5.2. Cophasing in Practice

For many years we have developed a flux and phase efficient method for white light fringe tracking by a double synchronous detection technique (Damé, 1996, Damé *et al*., 1997a, b).

A large spectral range (FWHM of 300 nm) is used to materialize coherence in reference interferometers working between non-repeated couples of telescopes of an array (e.g. 6 reference interferometers for 7 telescopes in an array). Because of the large spectral range only 5 significant fringes or so are present in the coherence domain (~ ± 2 µm), and with amplitude differences large enough for an easy identification of the central fringe for which the Optical Path Delay (OPD) nulling is effective (cf. Fig. 5).

The acquisition of interference fringes and the cophasing of an array are rather straightforward. Light is cut off the recombined beams either on a reference object (a reference star in the field) or on the object on a large, unused if possible, part of the spectrum (cf. Fig. 7). In the reference interferometers a modulation of the OPD is performed in one arm of each telescope couple with an amplitude of λ/2 or so. This allows to perform a synchronous detection at the same frequency than the modulation to obtain an error signal for the fringe centering (and phase control, in consequence). This is so because the synchronous detection is like a derivative where zeros of the function correspond to maxima. Another synchronous detection at double the frequency of modulation (a second derivative in some sense) reproduces the fringe pattern and allows to measure (while the system is already cophased on a fringe) the amplitude of that fringe. This double synchronous detection scheme allows, therefore, easily to locate the central fringe of OPD zero, ensuring the foreseen nulling of the system. This is explained in some details in our poster paper in these proceedings (Damé *et al*.., 1998, hereafter DDKM2); see Fig. 3 of DDKM2 for an illustration of the double synchronous detection acquisition and stabilization scheme on the central white-light fringe.

This method, applicable to the phasing of other interferometers or even large telescopes (like the NGST), has numerous advantages:

- a flux advantage since the bandpass is large (300 nm), allowing access to cophasing on reference sources as faint as a magnitude 10 for a peak-to-valley measured stability of yet λ/100 (cf. Damé *et al*., 1997, and DDKM2);
- a localized coherence zone allowing an unambiguous acquisition process of the fringes and subsequent cophasing (outside 2–3 times the coherence length — ± 5 µm in practice — there is no "coherent signal", i.e. no possible misleading of the cophasing acquisition process);
- the phase measure is not sensitive to pointing misalignments at first order, so that cross-talking between servo-controls is avoided (and residuals of pointing defects are not interpreted as cophasing ones...);
- stabilities up to λ/1000 or more are possible but the cophasing is also stable on low flux down to λ/4 or so, as shown in Damé *et al*., 1997a and DDKM2 (and this corresponds to the Rayleigh imaging criteria for "good images" up to the resolution limit).

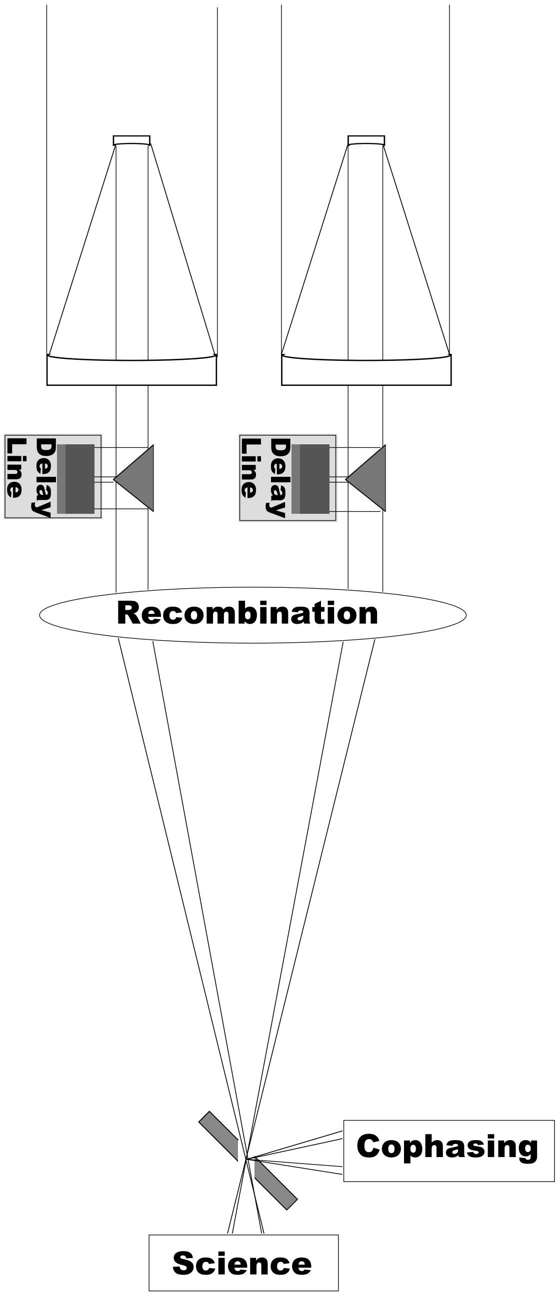

Figure 7. To each telescope or pupil segment is associated a delay line to phase the output beams. After recombination of the beams, e.g. at the level of an image of the field, a beamsplitter or field selector is introduced in order to take a reference source or spectrum to the cophasing system where phases between beams are measured (in order to control the optical path delays with the delay lines).

The method is currently demonstrated for two telescopes. Very soon (this summer) it will be implemented on a 3 telescopes' breadboard to demonstrate the complete imaging system (cf. DDKM2) and even tested on sky's objects (the Sun, Planets, stars) at Meudon Observatory this autumn (such tests on the sky were also carried successfully with the two telescope breadboard in 95 and 96). This Research and the Development Program of Space Interferometry Demonstration is supported by CNES since many years and was awarded recently a three years study (1998–2000). In this new program, spatialisation of the reference interferometers is foreseen starting with the three telescopes reference blocs (by molecular binding) of the SOLARNET interferometer (Fig. 8). A complete reference system for the cophasing of 3 telescopes should not exceed the size of a shoe box.

Let us recall that this measurement of the coherence degree (contrast) is done by controlling the scanning of a simple delay line so as to find the coherence zone (± 2 μm) where are the fringes. The coherence is materialized by a synchronous modulation of the path delay by another delay line at a reference frequency ν (300 Hz in practice) and with an amplitude of $\lambda/2$ or so (obtained by moving a retroreflector with a controlled piezoelectric), so that when we are in the coherence zone, the fringe position is shifted and, consequently, the intensity read on a detector where the fringes (flat tint in fact) are imaged in pupil plane (diodes of the external interferometer, cf. DDKM2). Two synchronous detections allow (at the reference frequency ν and at 2ν) to measure the shift (error signal required for the stabilization) but also its amplitude (so as to determine the best fringe: central one, highest positive one, *etc.*). A 20 000 lines of codes C++ program controls both the acquisition and the stabilization process since all instruments are linked to the computer by a GPIB/IEEE card (Frequency Generator, Synchronous Detections, Step Motors Electronic, Piezoelectric Amplifier, Computer Relays) and signals acquired (diodes and synchronous detections) monitored through by an acquisition card. Using the video clock of Windows 3.11 (in the multimedia library), treatment in within a modulation cycle (faster than 300 Hz) is achieved. Currently, we are undertaking a major upgrade of the program for use — starting this summer — with Win32 (NT 4) since preemptive multitasking and multithreading will bring very significant improvement allowing to control easily a multi- (5 to 7) telescopes setup.

Following the sky observations carried until last year (cf. Fig. 9 and Damé *et al.*, 1997b) we observed and cophased fringes on the Sun. Limited performance obtained in these early experiments ($\lambda/150$ or so) can be attributed to the lack of fine pointing (seeing is bad at Meudon, small fields are not always superimposed, and the small size of the refractor is sensitive to scintillation when observing stars); by September the SOLARNET breadboard will be upgraded to three telescopes and fine pointing (active mirrors) will be implemented.

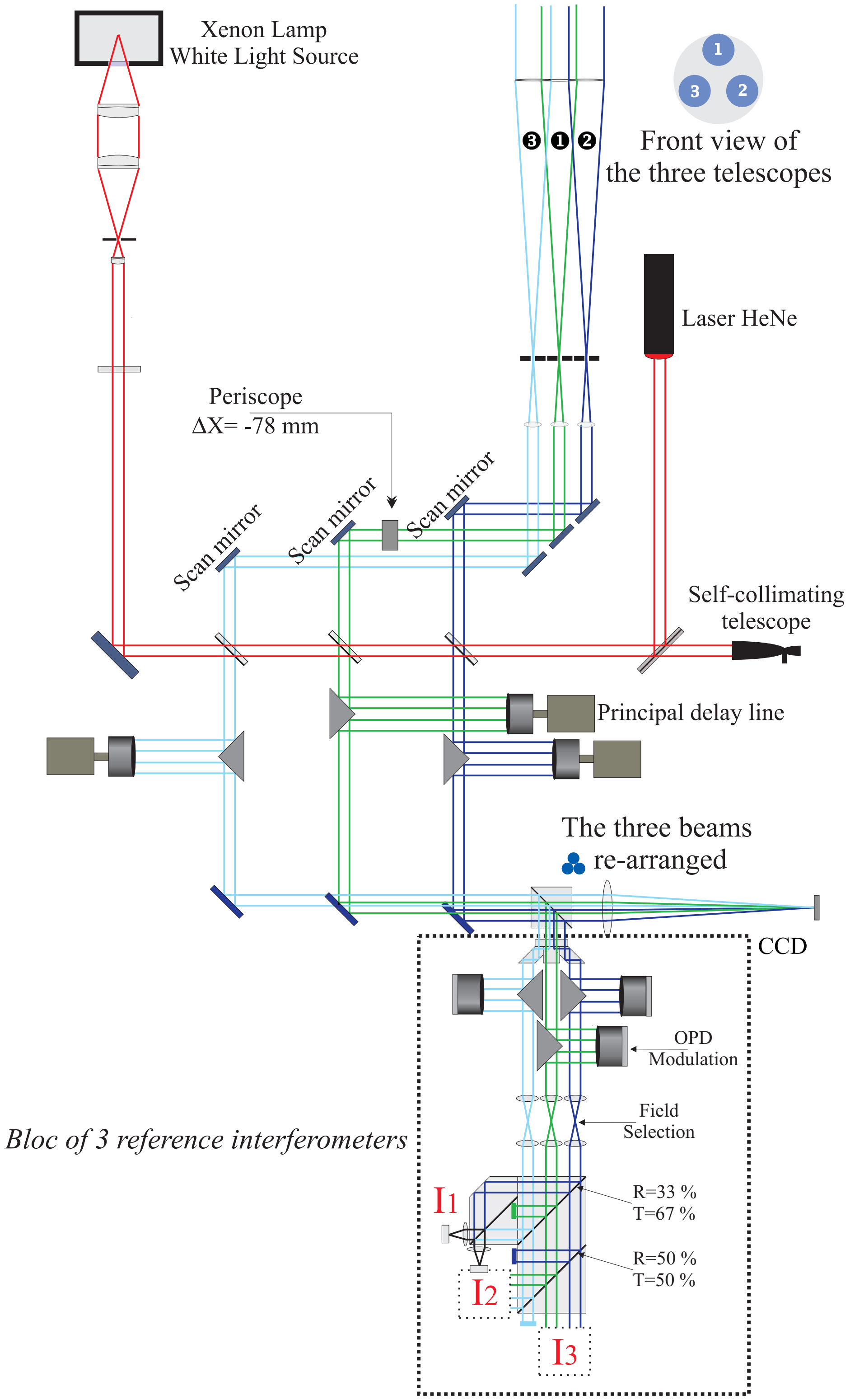

Figure 8. SOLARNET 3 telescopes imaging breadboard under realization at Service d'Aéronomie. The bloc (dash line) shows the 3 reference interferometers obtained by molecular binding. The bloc is not to scale and only partly representative (the third modulation delay line would be in the same plane than the others in a 3D view). The final realization (by mid-99) will be slightly more compact.

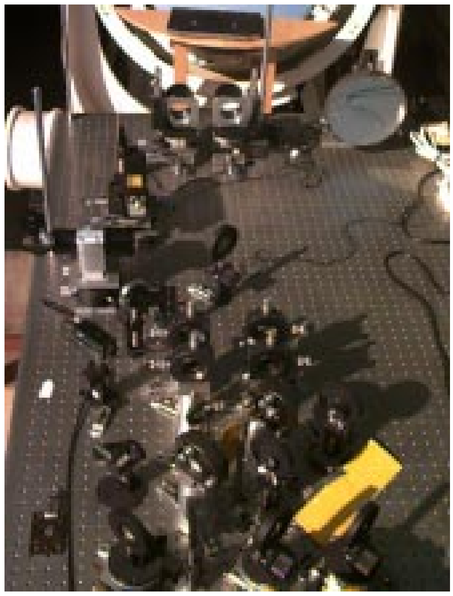

Figure 9. The 2 telescopes breadboard of SOLARNET during observations at the "Grand Sidérostat de Foucault" (a Ø800 mm mirror) at the Observatory of Meudon in March 1997.

Table 4. Minimum Model Payload of the Reduced SIMURIS Mission (for an ESA F2/F3 proposal involving the use of a PROTEUS platform several other instruments could be envisaged: EUV spectrograph, coronographs...).

Function	Instrument	Wavelength range (nm)	Spatial (arcsec) and spectral resolutions (nm)	Field-of-view ('': arcsec) (': arcmin)	Optical characteristics
High Spatial Resolution Imager	**SOLARNET (FUV-UV spectro-imaging)**	117 — 280 130 — 300 280 — 400	0.025" / 0.002 0.04" / ~ 20 0.06" / 0.001	40" x 40" 60" x 60" 60" x 60"	Three Ø35 cm Gregory telescopes on a baseline of 1 m followed by two double monochromators in cascade
High Temperature Imagers	**EUVT (Extreme Ultraviolet Telescopes)**	Fe XX/XXIII 13.3 Fe IX/X 17.3 Fe XII/XXI 19.2 Fe XIV 21.1	0.6" / ~ 1	5' x 5'	Ø10 cm Ritchey-Chrétien telescope with selectable multilayers
Large Field and Survey Imagers	**UVC (Ultraviolet Camera)** **HLT (Helium II Telescope)**	Lyman α 121.6 C IV 155.0 Continuum 160.0 He II 30.4	0.6" / ~ 10 0.6" / ~ 0.8 " 3" / ~ 1.5	2.5' x 2.5' Full Sun	Ø10 cm Gregory telescope with filter wheel (including a FP filter) Ø10 cm Ritchey-Chrétien telescope (multilayers)

6. DESIGN OF A SOLAR INTERFEROMETER

Fig. 10 summarizes the recombination and main optical characteristics of SOLARNET

SOLARNET is an interferometer made of 3 telescopes of Ø350 mm on a 1 m (950 mm) baseline. A general 3D view is given on Fig. 1 and a conceptual drawing of the optical layout is given in Fig. 10. The telescopes are Gregory systems, i.e. with an intermediate focus so as to eliminate most of the useless field-of-view (5 arcmin are kept for cophasing purpose and for the scientific field-of-view, 60"). The primary of the individual telescope is 350 mm in diameter opened at f/3 (focal of 1050 mm). The secondary mirror is 7 cm in diameter (focal of 21 cm). An optical layout of the telescope system and of the relay to the central recombining mirror is also indicated on Fig. 10. The recombining mirror (Ø190 and focal 1050 mm) localizes the light on the entrance slit (a 2 mm hole: 2D slit) of the scientific instrument (a subtractive double monochromator, SDM) where most of the field-of-view (5 arcmin minus the 60" that enter the SDM) is reflected towards the cophasing control system.

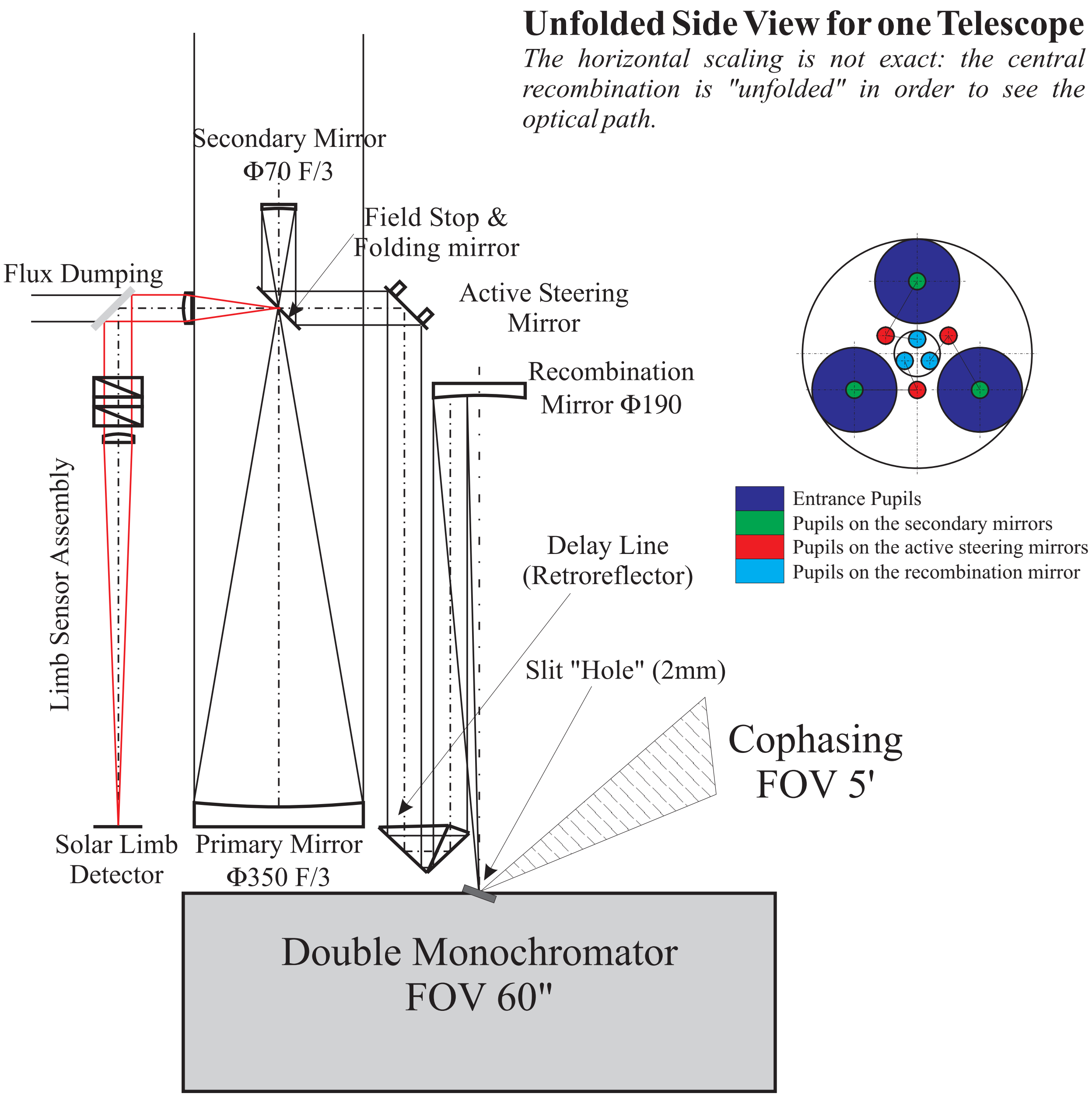

Figure 10. Design of SOLARNET (one of the 3 telescopes shown). Note the special use of relays at 30° to fit the recombination on a "small" 190 mm mirror, yet preserving a proper pupil orientation. Fine pointing is achieved on the solar limb taken off from the field stop inside the Gregory. The cophasing (by the delay lines) is monitored from a reference field feeding 3 reference interferometers directly from the entrance slit (2 mm hole) of the scientific instrument. Nothing is lost: 42 arcmin to pointing — 5 arcmin for cophasing — 1 arcmin for the scientific instrument.

Note that because the telescopes are near each other (for instantaneous image reconstruction high dynamics purpose) that the central telescope could not be the same size than the telescopes' primary but had to be smaller. For this reason, the arrangement of the active relay mirror and delay lines had to be rotated by 30° (cf. Fig. 10, left: configuration) so that the active mirrors do not block the light going back from the recombination mirror. By this original use of the 3D space, the recombination on the smaller Ø190 mm telescope is possible. It has the further advantage that an extra mechanism in output of the telescope can be added easily (as a polarizer for direct magnetic field measurement).

7. FOCAL INSTRUMENTATION

For the focal plane instrument a specific approach had to be developed since both spectral resolution and spectral bandwidth are required with the additional constraints that image reconstruction has to be performed. In practice, since based on Radio Interferometry methods, our image reconstruction simulations are working on filtergram type's data, i.e. on non-dispersed narrow bandpasses data. Adding spectral dispersion would produce extra complexity: overlapping fringes patterns — and their noise — over the 2D field at the different free wavelength bands allowed in the output. Interferometric imaging of complex and extended objects therefore requires the radio approach of limiting observations to narrow-band filtergrams. Note that in ground stellar optical interferometry the problem has not arisen since a slit usually selects a narrow field corresponding to the natural aperture angle of a speckle size (turbulence driven choice). In that case, it is a 1D field which gets to the spectrograph which subsequently disperses it. How to obtain such narrow bandwidths with grating spectrometers maintaining full two-dimensional imaging (no dispersion) and also tunability over a wide wavelength range? By use of a double monochromator in which the dispersions of the two gratings are subtractive. This concept has been studied in details up to the tolerance on the chromatic shear (cf. Damé *et al.*, 1993b). The principle of the Subtractive Double Monochromator (SDM) is illustrated on Fig. 11, where the first grating introduces the dispersion and the second one removes it while in the middle a slit selects, in image plane, the final spectral bandwidth. This system with two synchronous gratings provides also stray light protection and easy field selection. While not necessary for point sources (Astrophysics) this system, capable of instantaneous 2D-imaging, will also find applications in earth observation systems and military programs.

The SDM that we propose uses the full potential of the approach by providing, in addition, simultaneous outputs in cascade, tunable from the far UV (117 nm) to the visible (400 nm). For this, two SDM are used in cascade. This is achieved by a Wadsworth mounting of the first grating. This optical set up (cf. Fig. 12), often used is small spectrometers, has the advantage that the output beam has a fixed direction (the exit slit is fixed). In our case, it allows the zero order reflected by the first grating of the far UV SDM to enter a second SDM (200 — 400 nm range, cf. Table 5). The input beam to the second stage is fixed while the far UV SDM scans its spectral range. By this approach, several channels are observable simultaneously with a completely free choice of the lines in each of them: they are fully independent.

Even though it might appear of some complexity (cf. the optical layout, Fig. 13), this is the only way by which interferometric imaging can presently be achieved with spectral resolution of 0.01 to 0.1 nm and in different lines simultaneously.

The SDM implementation was studied in details for the SUN and MUST concepts (Kruizinga *et al.*, 1992, Damé *et al.*, 1993b) and adapted to SOLARNET.

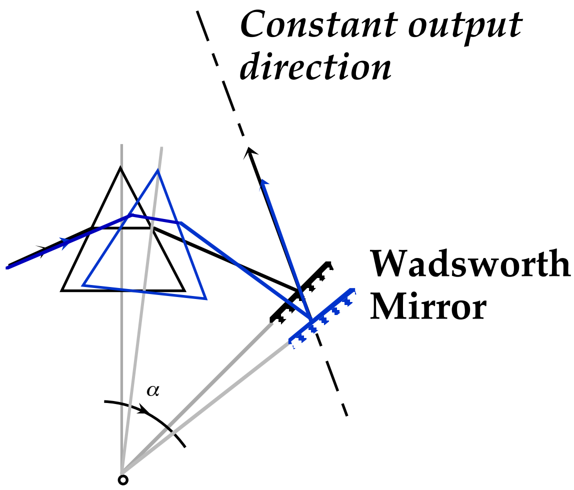

Figure 12. Illustration of the function of a Wadsworth flat relay mirror for the zero order. Moving the prism (grating) - i.e. selecting lines — does not affect the output direction of the beam (allowing to fed a second double monochromator with the zero order).

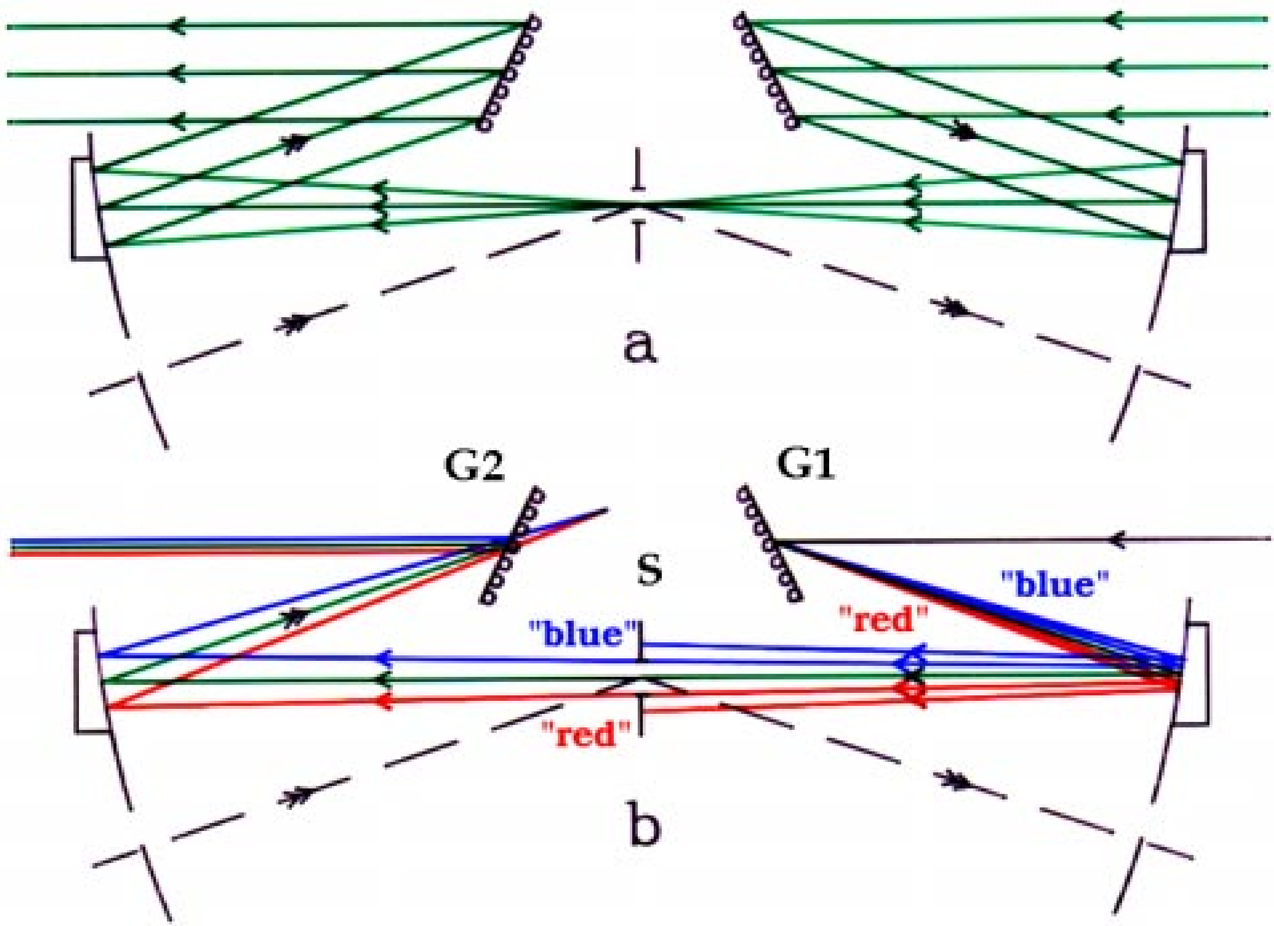

Figure 11. Principle of the Double Monochromator of the SOLARNET Interferometer: optical (a) and spectral (b). The first grating (G1) disperses the light which is recombined by the second grating (G2) after a spectral selection, in image plane, done by an intermediate slit (S).

8. RESOURCES SUMMARY

This simplified version of SOLARNET with only 3 telescopes of Ø350 mm was first envisaged for the Space Station. This basic system will allow to test the cophasing techniques and a possible pointing influence with, if necessary, access to one closure phase. Additional advantages of this configuration are the reduced number of optics and the 3-telescopes recombination since larger interferometers in Space (diluted for Astrophysics needs) will probably measure phases by recombining beams three by three. This three by three recombination is not required for Imaging Interferometers (either solar, planetary, military or dedicated to earth observations) which will be compact (full spatial frequencies coverage achieved instantaneously) and, more efficiently, will recombine directly all beams together to get an extended field-of-view image.

For interferometric technologies demonstration SOLARNET on a SMART or on the Space Station will require a primary pointing to half a degree or so (from the platform for the SMART; from an Hexapod, 6 linear actuators, on the Space Station). Internal fine pointing will allow to reach the tens of mas required for interferometric purpose.

A third technology that we will study with SOLARNET

Table 5. Characteristics (spatial and spectral) of SOLARNET focal plan instrumentation.

Wavelength range (nm)	Field-of-view (arcsec)	Detectors		Spatial resolution (arcsec)	Spectral resolution (nm)
		pixels	Type		
FUV: 117 — 200 130 — 300	40 x 40 60 x 60	2048 x 2048	CCD	0.025 — 0.04 0.04 — 0.1	0.002 ~ 20
UV: 280 — 400	60 x 60	2048 x 2048	CCD	0.06 — 0.08	0.01 (0.001*)

* This could be achieved with an extra filtering (Fabry-Perot)

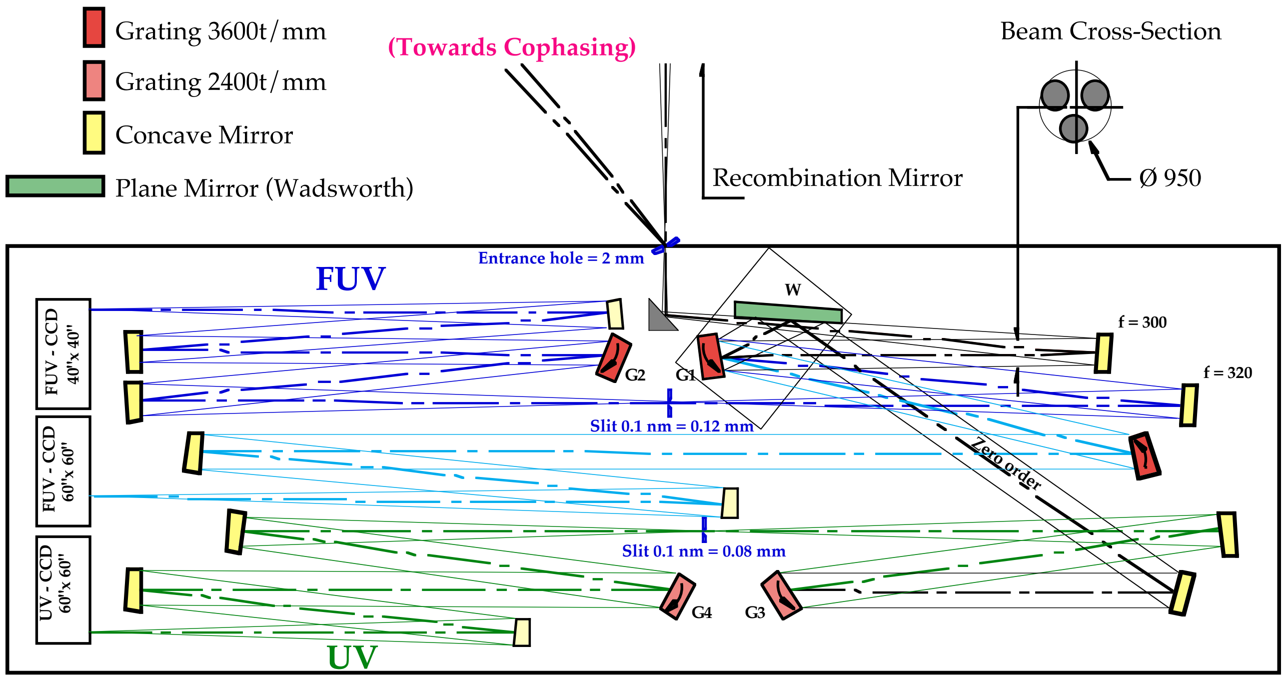

Figure 13. Configuration of the Subtractive Double Monochromator (SDM) of SOLARNET. Note, in particular, the sets of double gratings (G1,G2) and (G3,G4). They rotate synchronously to compensate for the spectral dispersion. The second SDM is fed by a flat mirror (W) linked to the first grating (G1) which has the particularity to send the zero order always in the same direction (Wadworth's mount).

is lightweight telescopes. The three 35 cm telescopes of SOLARNET will represent only 24 to 30 kg. This is possible since the real-time active pointing and cophasing, relax the inertial tolerances on the stability of the telescopes. The active systems will compensate for the lack of rigidity of the structure.

The technologies tests that SOLARNET will provide are important to many of the currently envisaged mission concepts for high resolution astronomy: cf. the proceedings of the Symposium on *Scientific Satellites Achievements and Prospects in Europe*, 1996, edited by the AAAF. More than half of the new mission concepts presented at this Symposium were interferometers!
Table 6 summarizes the SOLARNET required resources. Our mass evaluation includes a 20 % contingency. Telemetry is voluntarily limited by use of onboard (non-destructive) data compression. Compression factors of 4 to 6 can be envisaged without losses and, since progress in this domain happens rapidly, a factor of 10 could be considered for a flight in 2004–2006.

9. CONCLUSION

At the end of this paper, and taking into account the sustained R & D program of this year (3 telescopes imaging breadboard with fine pointing, phase control and image reconstruction on the Sun and Planets), we believe that an imaging interferometer is *not at all* premature as a very serious candidate for the major instrument of the next ESA solar mission (F2/F3 opportunity). We proved that the major assumption of the overall concept, the cophasing of the array, is feasi-

Table 6. SOLARNET resources summary.

Mass	160 kg (including 20% margin)
Telemetry	100 kbits/s average (4 Mbits/s at maximum rate)
Envelope	Ø110 x 150 cm^3 (3 x Ø35 cm telescopes)
Primary pointing accuracy	0.5°
Primary pointing stability	0.03°/s
Secondary (active) pointing stability	≤ 12 milliarcsec
Internal phase control	≤ $\lambda/8$ (at Lyman α, 120 nm)
Field-of-view	1.2° (Sun viewing)
Power	60 watts (peak: 75 watts)
Mission duration	3 to 6 years

ble and, moreover, that performances to expect are very high. SOLARNET will not only provide breakthrough science with a spatial resolution in the UV 40 times better than anything flown — 0.02" spatial resolution on a 40" FOV — but also at an incredibly low cost because of the compactness of the interferometric concept allowing the use of a standard, industrial, platform like the CNES/AEROSPATIALE PROTEUS one. This should be a clear signal to the solar community that new Physics can come from new technologies readily available, and that a Mission with a 1 meter equivalent telescope could be made around interferometry in the coming years, much earlier — and much easier — that most people would have thought of. Furthermore, this first interferometer in Space will serve as a technology demonstration of interferometric techniques for the future — larger — Space Interferometry Missions or, even, the phasing of the NGST. More details on the instrument and mission scenario, cophasing techniques, image reconstruction algorithms, double monochromator design and spectral performances, and our laboratory and "sky" results are — and will be — available on our Web server:

http://must.aerov.jussieu.fr/solarnet_facts.htm.

10. ACKNOWLEDGMENTS

We would like to mention the contributions of Renée Prangé, Philippe Zarka and Anny-Chantal Levasseur-Regourd for the solar system scientific objectives. This work is partly supported by CNES R & T Grants since 92 and benefited from an ESA TRP contract for implementing part of the new 3 telescopes breadboard under realization. We are grateful to MATRA MARCONI SPACE for financial support in 94 and 95 that allowed to complete the two-telescopes breadboard and to carry the solar tests at Meudon Observatory.

11. REFERENCES

Allen, M.J. *et al.*: 1997, Chromospheric and Coronal Structure of Polar Plumes, Sol. Phys. **174**, 367

Ben Jaffel, L., J.T. Clarke, R. Prangé, R.Gladstone, A. Vidal-Madjar, A.: 1993, The Lyman α bulge of Jupiter: Evidence of non-thermal effects, Geophys. Res. Lett. **20**, 747-750

Connerney, J. E. P., R. Baron, T. Satoh and T. Owen: 1993, Images of excited H_3^+ at the foot of the Io flux tube in Jupiter's atmosphere, Science **262**, 1035-1038

Coradini, M., Damé, L. *et al.*: 1991, Solar, Solar System and Stellar Interferometric Mission for Ultrahigh Resolution Imaging and Spectroscopy (SIMURIS), Scientific and Technical Study — Phase I, ESA Report SCI(91)7

Cornwell, T.J., Holdaway, M.A. and Uson, J.M.: 1993, Radio-interferometric imaging of large objects: implications for array design, Astron. Astrophys. **271**, 697

Damé, L.: 1998, Low Orbit High Resolution Solar Physics with the Solar Interferometer, Adv. Space Res. **21**(1/2), 295–304

Damé, L., Derrien, M., Kozlowski, M. and Merdjane, M.: 1998, Laboratory and Sky Demonstrations of Solar Interferometry Possibilities, these proceedings (DDKM2)

Damé, L.: 1997, A revolutionary concept for high resolution solar physics: solar interferometry, ESA Symposium on *Scientific Satellites Achievements and Prospects in Europe*, Ed. AAAF, 3.31-3.43

Damé, L., Derrien, M., Kozlowski, M., Merdjane, M. and Clavel, B.: 1997a, Investigation of the low flux servo-controlled limit of a cophased interferometer, CNES International Conference on *Space Optics (ICSO'97)*, Ed. G. Otrio, S2

Damé, L., Hersé, M., Kozlowski, M., Martić, M., Merdjane, M. and Moity, J.: 1997b, Solar interferometry: a revolutionary concept for high resolution solar physics, in *Forum THEMIS — Science with THEMIS*, Publication de l'Observatoire de Paris-Meudon, Eds. N. Mein and S. Sahal-Bréchot, 187–200

Damé, L.: 1996, The MUST/3T Solar Interferometer: an Interferometric Technologies TestBed on the International Space Station", ESA Symp. on Space Station Utilization, Darmstadt, 30 Sept.–2 Oct. 1996, Ed. T.D. Guyenne, ESA SP-**385**, 369

Damé, L., Derrien, M., Kozlowski, M. and Ruilier, C.: 1995, Instrumental Prospects in Solar Interferometric Imaging, 27th JOSO Meeting, Benesov, Tcheque Republic, 12–15 November 1995, JOSO Annual Report 1995, 52-59

Damé, L.: 1994, Solar Interferometry: Space and Ground Prospects, in *Amplitude and Intensity Spatial Interferometry II*, Ed. J.B. Breckinridge, Proc. SPIE–**2200**, 35–50

Damé, L.: 1993, Actively Cophased Interferometry with SUN/SIMURIS, in *Spaceborne Interferometry,* Ed. R.D. Reasenberg, Orlando, Proc. SPIE–**1947**, 161

Damé, L. *et al.*: 1993a, A Solar Interferometric Mission for Ultrahigh Resolution Imaging and Spectroscopy (SIMURIS), Proposal to ESA Call for the "Next Medium Size Mission — M3"

Damé, L., Martić, M. and Rutten, R.J.: 1993b, Prospects for Very-High-Resolution Solar Physics with the SIMURIS Interferometric Mission, in *Scientific Requirements for Future Solar Physics Space Missions*, Ed. B. Battrick, ESA SP-**1157**, 119–144

Damé, L.: 1992, Demonstration and Performances of Real-Time Fringe Tracking: a Step Towards Cophased Interferometers, in *Solar Physics and Astrophysics at Interferometric Resolution*, Eds. L. Damé and T.D. Guyenne, ESA SP–**344**, 277

Damé, L. and Cornwell, T.J.: 1992, Interferometric Imaging with the Solar Ultraviolet Network, In ESA Workshop on *Solar Plysics and Astrophysics at Interferometric Resolution*, Eds. L. Damé and T.D. Guyenne, ESA SP-**344**, 185

Damé, L. *et al.*: 1989, A Solar Interferometric Mission for Ultrahigh Resolution Imaging and Spectroscopy

(SIMURIS), Proposal to ESA Call for the "Next Medium Size Mission — M2"

Damé, L. and Vakili, F.: 1984, The Ultra Violet Resolution of Large Mirrors via Hartmann Tests and Two Dimensional Fast Fourier Transform Analysis, *Optical Eng*. **23**(6), 759

Emerich, C., Ben Jaffel, L., Clarke, J.T., Prangé, R., Sommeria, J., Gladstone, G.R. and Ballester, G.E.: 1996, Detection of supersonic motions in the upper atmosphere of Jupiter, Science **273**, 1085

Hanner, M.S., Hackwell, J.A., Russel, R.W., Lynch, D.K.: 1994, Icarus **112**, 490

Hudson, H.S. *et al*.: 1994, Analysis of Three YOHKOH White-Light Flares, Proc. of Kofu Symposium, Eds. S. Enome and T. Hirayama, NRO Report **360**, 397

Kruizinga, B. *et al*.: 1992, The Solar Ultraviolet Network Subtractive Double Monochromator, ESA Workshop on *Solar Physics and Astrophysics at Interferometric Resolution*, Eds. L. Damé and T.D. Guyenne, ESA **SP-344**, 181

Levasseur-Regourd, A.C., Hadamcik, E. and Renard, J.B.: 1996, Astron. Astrophys. **313**, 327

Mein, N., Mein, P. and Wijk, J.E.: 1994, Dynamical fine structure of a quiescent filament, Sol. Phys. **151**, 75

Pojoga, S., Nikoghossian, A.G. and Mouradian, Z.: 1998, A statistical approach to the investigation of fine structure of solar prominences, Astron. Astrophys. **332**, 325

Porter, J. *et al*.: 1994, Microflaring at the feet of large active regions loops, Proc. of Kofu Symposium, Eds. S. Enome and T. Hirayama, NRO Report **360**, 65

Prangé, R.: 1992, Magnetospheres and Atmospheres of Planets, Proceedings Workshop ESA*Solar Physics and Astrophysics at Interferometric Resolution,* Eds. L. Damé and T.D. Guyenne, ESA-SP **344**, 131-138

Prangé, R. and Zarka, P.: 1993 (October), J3S: Jupiter and Saturn Systems Survey, response to ESA call for *Post-Horizon 2000*" mission concepts

Prangé, R., D. Rego and J.C. Gérard: 1995, Lyman α and H_2 bands from the giant planets: 2. Effect of the anisotropy of precipitating particles on the interpretation of the 'color ratio' of Jovian aurorae, J. Geophys. Res. **100**, 7513

Pallier, L. *et al*.: 1997, HST spectro-imaging of Jupiter's aurorae with FOC and GHRS, in relation with Galileo in-situ measurements, DPS Meeting **29**, 16.08

Priest, E.R., Foley C.R., Heyvaerts, J., Arber, M., Culhane, J.L. and Acton, L.W.: 1998, Ap. J. (submitted)

Rego, D., Prangé, R. and Gérard, J.C.: 1994, Lyman α and H_2 bands from the giant planets: 1. Excitation by proton precipitation in the Jovian aurorae, J. Geophys. Res. **99**, 17075-17094

Sommeria, J., Ben Jaffel, L. and Prangé, R.: 1995, On the existence of supersonic jet generation in the auroral upper atmosphere of Jupiter**,** Icarus **199**, 2

Veverka, J. *et al*.: 1997, NEAR's Flyby of 253 Mathilde: Images of a C Asteroid, Science **278**, 2109

Vial, J.-C., Rovira, M., Fontenla, J. and Gouttebroze, P.: 1989, Multithread structure as a possible solution for the Lyman ß problem in solar prominences, Proceedings of Colloquium 117, Hvar Observatory Bulletin **13**, 47

Yeomans, D.K. *et al*.: 1997, Estimating the Mass of Asteroid 253 Mathilde from Tracking Data During the NEAR Flyby, Science **278**, 2106

Zarka, P. *et al*.: 1996, ISS/J3S: *Global Long-Term Multispectral Monitoring of Jupiter and Saturn Magnetospheres*, ESA SP-**385**, 10

Zarka, P.: 1992, The auroral radio emissions from planetary magnetospheres, *Adv. Space Res*., **12**(8), 99-115